Band Gaps of the Lead-Free Halide Double Perovskites $Cs_2BiAgCl_6$ and $Cs_2BiAgBr_6$ from Theory and Experiment

Supporting Information

Marina R. Filip,[†] Samuel Hillman,[‡] Amir Abbas Haghighirad,[‡] Henry J. Snaith,[‡] and Feliciano Giustino[*,†]

Department of Materials, University of Oxford, Parks Road OX1 3PH, Oxford, UK, and Department of Physics, University of Oxford, Clarendon Laboratory, Parks Road, Oxford OX1 3PU, UK

E-mail: feliciano.giustino@materials.ox.ac.uk

[*]To whom correspondence should be addressed
[†]Department of Materials, University of Oxford
[‡]Department of Physics, University of Oxford

Computational Setup

Band structure and density of states calculations. All density functional theory calculations are performed within the local density approximation (LDA),[1] as implemented in the `Quantum Espresso` suite.[2] Band structures are calculated with and without spin-orbit coupling effects, using ultrasoft pseudopotentials[3] including non-linear core correction[4] for Bi, Ag, Cl and Br, as found in the Theos Library.[5] For Cs we use the norm-conserving non-relativistic pseudopotential in the Quantum Espresso Library. For the projected density of states we sample the Brillouin zone using a dense $20 \times 20 \times 20$ k-point grid in both cases. The molecular orbital diagrams shown in Figure 2a are built using the data obtained from the projected density of states calculations. For the band structure and projected density of states calculations we use plane-wave cutoffs of 60 Ry and 300 Ry for the wave functions and charge density respectively.

Ground state calculations. For the calculation of the single particle energies, we use norm-conserving[6] pseudopotentials. For Cs and Cl we use non-relativistic pseudopotentials (as found in the Quantum Espresso library) as we do not expect the spin-orbit coupling effects to be significant for these ions. In the case of Bi, Ag and Br we generated a set of fully relativistic, Troullier-Martins norm conserving pseudopotentials[6] using the `ld1.x` code of the Quantum Espresso distribution. For these ions we consider the following electronic configurations: $5d^{10}6s^26p^3$ (Bi), $4s^24p^64d^{10}5s^0$ (Ag) and $3d^{10}4s^24p^5$ (Br). In order to show the importance of semicore electrons for GW calculations we also generate a pseudopotential of Ag with the $4d^{10}5s^1$ configuration. Unless otherwise specified, all calculations are performed including semicore states for Ag. The charge density is calculated using a large plane wave cutoff of 300 Ry and a $10\times10\times10$ Γ-centred k-point grid in order to sample the Brillouin zone.

Quasiparticle energies. The quasiparticle energies can be calculated from many-body perturbation theory as: $E_{n\mathbf{k}} = \epsilon_{n\mathbf{k}} + Z(\epsilon_{n\mathbf{k}})\langle n\mathbf{k}|\Sigma_{n\mathbf{k}}(\epsilon_{n\mathbf{k}}) - V_{\mathrm{xc}}|n\mathbf{k}\rangle$,[7–10] where $\epsilon_{n\mathbf{k}}$ are the Kohn-

Sham eigenvalues for band n and wave-vector $\mathbf{k}$, $E_{n\mathbf{k}}$ are the corresponding eigenvalues, $\Sigma(\omega)$ is the frequency-dependent self-energy, $Z(\omega) = [1 - \mathrm{Re}(\partial\Sigma/\partial\omega)]^{-1}$ is the quasiparticle renormalization, and V_{xc} is the exchange and correlation potential. The self-energy is calculated within the G_0W_0 approximation as $\Sigma = \mathrm{i}G_0W_0$, where G_0 is the single-particle Green's function and W_0 is the screened Coulomb interaction. The self energy is typically separated into two terms, the energy-independent exchange self energy, Σ_{x}, and the energy dependent correlation self energy, Σ_{c}.[7–10]

For the calculation of the quasiparticle eigenvalues we use the G_0W_0 approximation as implemented in the `Yambo` code.[11] We calculate the dielectric matrix within the random phase approximation[12,13] and model its frequency dependence within the Godby-Needs plasmon pole approximation.[14] We use a plane wave cutoff of 50 Ry ($Cs_2BiAgCl_6$) and 60 Ry ($Cs_2BiAgBr_6$) to calculate the exchange part of the self-energy.

In Figures S4 and S5 we show the convergence with respect to the empty states and polarizability cutoff of the direct band gaps calculated at the Γ-point for $Cs_2BiAgCl_6$ and $Cs_2BiAgBr_6$ respectively. We have also checked that the indirect band gaps follow a similar convergence trend. We define the empty states cutoff as the energy of the highest band included in the summation over empty states with respect to the valence band top at the Γ-point. The points at the top right corner of Figures S4a and S4b correspond to calculations which include 1000 total bands (906 empty states in the case of $Cs_2BiAgCl_6$ and 856 empty states in the case of $Cs_2BiAgBr_6$). We find that the band gap converges within 20 meV for 600 bands and 95 eV cutoff in both cases. In addition, we test the convergence with respect to the $\mathbf{k}$-point mesh. We obtain that the band gap at Γ point of $Cs_2BiAgCl_6$ changes by 10 meV when we increase the density of the $\mathbf{k}$-point mesh from a $4 \times 4 \times 4$ grid to a $5 \times 5 \times 5$ grid.

The final set of parameters used for our best converged calculation is: 50 Ry ($Cs_2BiAgCl_6$) and 60 Ry ($Cs_2BiAgBr_6$) plane-wave cutoff for the exchange self energy, 600 bands, 95 eV

plane-wave cutoff for the polarizability and a $4 \times 4 \times 4$ **k**-point mesh centred at Γ.

Experimental Methods

Solution-based synthesis and crystal growth of Cs_2BiAgX_6 (X = Cl, Br). Samples of Cs_2BiAgX_6 (X= Cl, Br) were prepared by precipitation from an acidic solution of hydrochloric and hyrobromic acid. A mixture of a 1 mmol $BiBr_3$ (Sigma Aldrich, 99.99%) and AgBr (Sigma Aldrich, 99%) were first dissolved in 12 ml 8.84 M HBr. 2 mmol of CsBr (Sigma Aldrich, 99.9%) were added and the solution was heated to 150°C to dissolve the salts. The solution was cooled to 118°C at 4°C/hour to initiate supersaturation and produce single crystals. The chlorine compound $Cs_2BiAgCl_6$ was fabricated using similar solution method with hydrochloric acid, $BiCl_3$ and CsCl.

High-purity polycrystalline samples were synthesised following the method used by McClure2016 et al.[15] A mixture of 8 ml (8.84 M) HBr and 2 ml 50 wt% H_3PO_2 solution was heated to 120°C and 1.31 mmol of AgBr and $BiBr_3$ dissolved into it. Adding 2.82 mmol of CsBr caused an orange precipitate to form immediately. The hot solution was left for 30 minutes under gentle stirring to ensure a complete reaction before being filtered and the resulting solid washed with ethanol and dried in a furnace.

Synthesis via solid-state reaction. Single-phase samples of Cs_2BiAgX_6 (X = Cl, Br) were prepared by conventional solid-state reaction in a sealed fused silica ampoule.[16] For a typical reaction, the starting materials CsCl, CsBr (Sigma Aldrich, 99.9%), $BiCl_3$, $BiBr_3$ (Sigma Aldrich, 99.99%) and AgCl, AgBr (Sigma Aldrich, 99%) were mixed in a molar ratio 2:1:1, respectively. The mixture was loaded in a fused silica ampoule that was flame sealed under vacuum (10-3 Torr). The mixture was heated to 500°C over 5 hours and held at 500°C for 4 hours. After cooling to room temperature, a yellow and orange polycrystalline material was formed for $Cs_2BiAgCl_6$ and $Cs_2BiAgBr_6$, respectively. Octahedral shaped crystals of maximum size 1 mm^3 could be extracted from the powder samples that later were used to determine the crystal structures.

Structural characterization. Powder X-ray diffraction was carried out using a Panalytical X′pert powder diffractometer (Cu-$K_{\alpha 1}$ radiation; λ = 154.05 pm) at room temperature. Structural parameters were obtained by Rietveld refinement using General Structural Analysis Software.[17] Single crystal data were collected for $Cs_2BiAgCl_6$ and $Cs_2BiAgBr_6$ at room temperature using an Agilent Supernova diffractometer that uses Mo K_α beam with λ = 71.073 pm and is fitted with an Atlas detector. Data integration and cell refinement was performed using CrysAlis Pro Software (Agilent Technologies Ltd., Yarnton, Oxfordshire, England). The structure was analysed by Patterson and Direct methods and refined using SHELXL 2014 software package.[18]

Optical characterization. A Varian Cary 300 UV-Vis spectrophotometer with an integrating sphere was used to acquire absorbance spectra and to account for reflection and scattering. A 397.7 nm laser diode (Pico-Quant LDH P-C-405) was used for photoexcitation and pulsed at frequencies ranging from 1-80 MHz. The steady-state photoluminescence (PL) measurements were taken using an automated spectrofluorometer (Fluorolog, Horiba Jobin-Yvon), with a 450 W-Xenon lamp excitation.

Table S1: Crystallographic data for a $Cs_2BiAgCl_6$ single crystal. The refinement data are the same as those we reported in Table S1 of the Supporting Information of Ref.[16]

Compound	$Cs_2BiAgCl_6$
Measurement temperature	293 K
Crystal system	Cubic
Space group	$Fm\bar{3}m$
Unit cell dimensions	a = 10.777 ± 0.005 Å
	$\alpha = \beta = \gamma = 90°$
Volume	1251.68 $Å^3$
Z	4
Density (calculated)	4.221 g/cm^3
Reflections collected	3434
Unique reflections	82 from which 0 suppressed
R(int)	0.1109
R (sigma)	0.0266
Goodness-of-fit	1.151
Final R indices (R_{all})	0.0212
wR_{obs}	0.0322
Wavelength	0.71073 Å
Weight scheme for the refinement	Weight = 1/[sigma^2(Fo^2)+(0.0074 * P)^2+0.00*P] where P = (Max(Fo^2,0)+2*Fc^2)/3
Isotropic temperature factors (Å^2)	U_{iso} (Cs) 0.04284 ± 0.00044, (Bi) 0.02103 ± 0.00040 , (Ag) 0.02384 ± 0.00048, (Cl) 0.05063 ± 0.00107
Anisotropic temperature factor (Å^2)	U_{11}(Cs) = 0.04284 ± 0.00044, U_{11}(Bi) = 0.02103 ± 0.00040, U_{11}(Ag) = 0.02384 ± 0.00048, U_{11}(Cl) = 0.02039 ± 0.00149, U_{22}(Cs) = 0.04248 ± 0.00044, U_{22}(Bi) = 0.02103 ± 0.00040, U_{22}(Ag) = 0.02384 ± 0.00048, U_{22}(Cl) = 0.06567 ± 0.00152, U_{33}(Cs) = 0.04248 ± 0.00044, U_{33}(Bi) = 0.02103 ± 0.00040, U_{33}(Ag) = 0.02384 ± 0.00048, U_{33}(Cl) = 0.06567 ± 0.00152

Atomic Wyckoff-positions	Atom	Site	x	y	z	site occupancy
	Cs	8c	0.25	0.25	0.25	1
	Bi	4a	0	0	0	1
	Ag	4b	0.5	0.5	0.5	1
	Cl	24e	0.2489	0	0	1

Table S2: Crystallographic data for a $Cs_2BiAgBr_6$ single crystal.

Compound	$Cs_2BiAgBr_6$
Measurement temperature	293 K
Crystal system	Cubic
Space group	$Fm\bar{3}m$
Unit cell dimensions	a = 11.264 ± 0.005 Å
	$\alpha = \beta = \gamma = 90°$
Volume	1429.15 $Å^3$
Z	4
Density (calculated)	4.936 g/cm^3
Reflections collected	3830
Unique reflections	95 from which 0 suppressed
R(int)	0.0691
R (sigma)	0.0150
Goodness-of-fit	0.369
Final R indices (R_{all})	0.0192
wR_{obs}	0.0676
Wavelength	0.71073 Å
Weight scheme for the refinement	Weight = 1/[sigma^2(Fo^2)+(0.1874 * P)^2+0.00*P] where P = (Max(Fo^2,0)+2*Fc^2)/3
Isotropic temperature factors ($Å^2$)	U_{iso} (Cs) 0.05012 ± 0.00077, (Bi) 0.01985 ± 0.00051 , (Ag) 0.02820 ± 0.00071, (Br) 0.05347 ± 0.00066
Anisotropic temperature factor ($Å^2$)	U_{11}(Cs) = 0.05012 ± 0.00077, U_{11}(Bi) = 0.01985 ± 0.00051, U_{11}(Ag) = 0.02820 ± 0.00071, U_{11}(Br) = 0.02003 ± 0.00092, U_{22}(Cs) = 0.05012 ± 0.00077, U_{22}(Bi) = 0.01985 ± 0.00051, U_{22}(Ag) = 0.02137 ± 0.00296, U_{22}(Br) = 0.07019 ± 0.00083, U_{33}(Cs) = 0.05012 ± 0.00071, U_{33}(Bi) = 0.01985 ± 0.00051, U_{33}(Ag) = 0.02137 ± 0.00296, U_{33}(Br) = 0.07019 ± 0.00083

Atomic Wyckoff-positions

Atom	Site	x	y	z	site occupancy
Cs	8c	0.25	0.25	0.25	1
Bi	4a	0	0	0	1
Ag	4b	0.5	0.5	0.5	1
Br	24e	0.25091	0	0	1

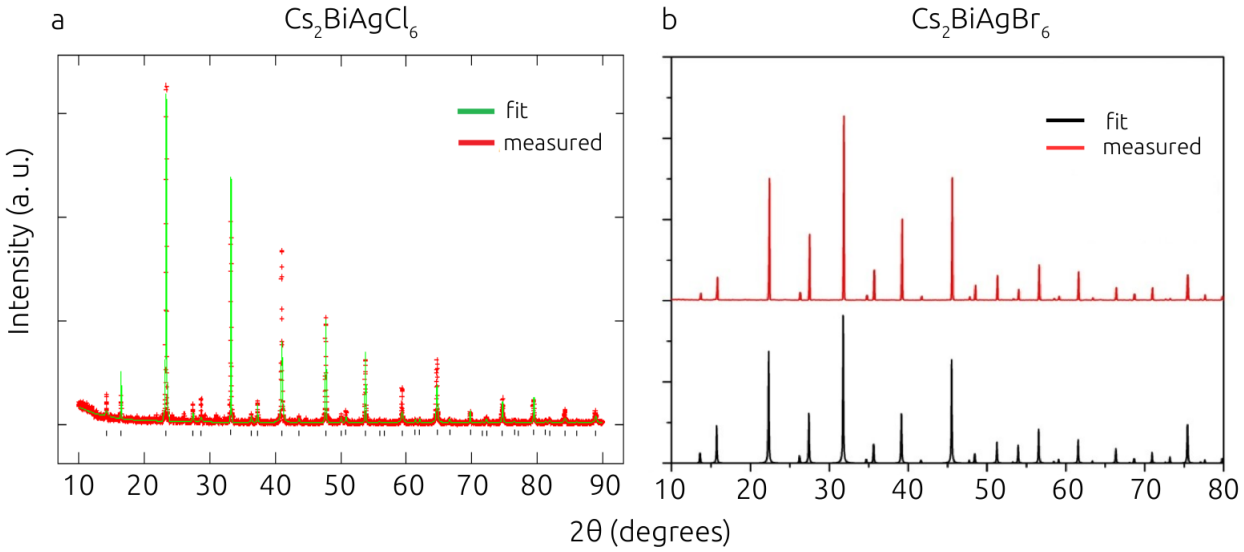

Figure S1: Powder X-ray diffraction spectrum for of $Cs_2BiAgCl_6$ (a) and $Cs_2BiAgBr_6$ (b) measured at room temperature. The spectrum in (a) is the same as we obtained in Figure S6 of the Supporting Information of Ref[16]

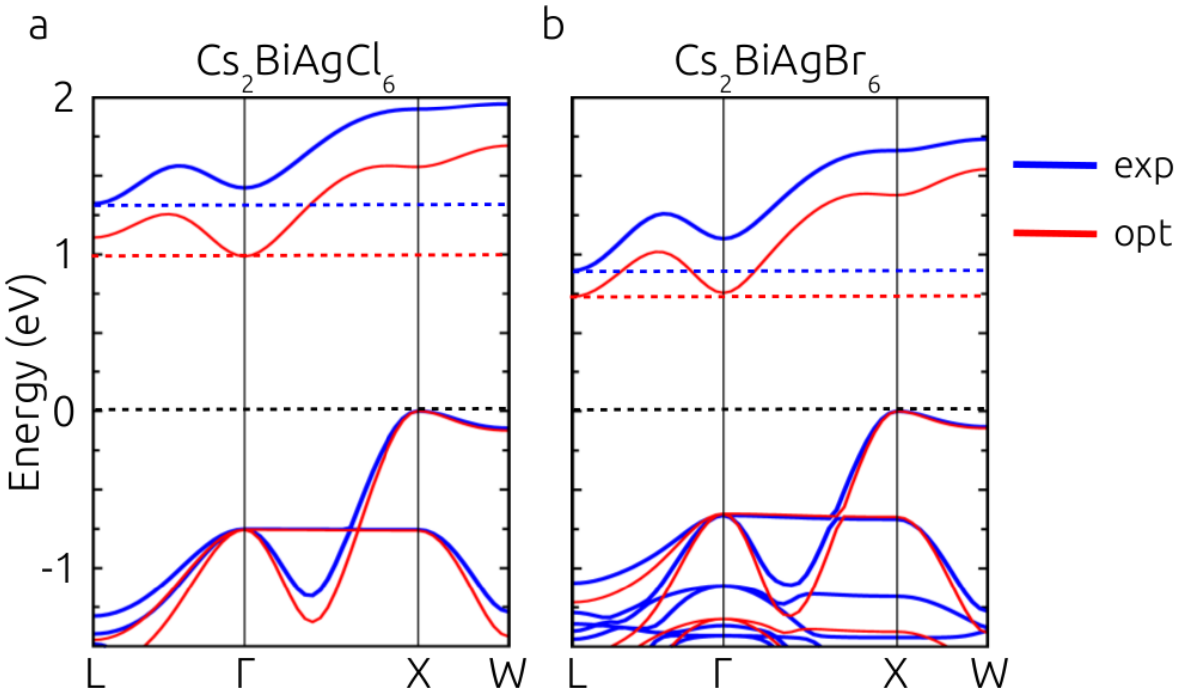

Figure S2: Comparison between the band structures of $Cs_2BiAgCl_6$ (a) and $Cs_2BiAgBr_6$ (b) calculated for the experimental (exp) crystal structures reported in Ref.[16] ($Cs_2BiAgCl_6$) and in Table S1 ($Cs_2BiAgBr_6$) and the optimized (opt) crystal structures. The dashed lines indicate the band edges (black for the valence band top in each case, red and blue for the conduction band bottom obtained from the calculation on the optimized and experimental crystal structures, respectively). The optimized crystal structures are obtained as described in Ref.[16]

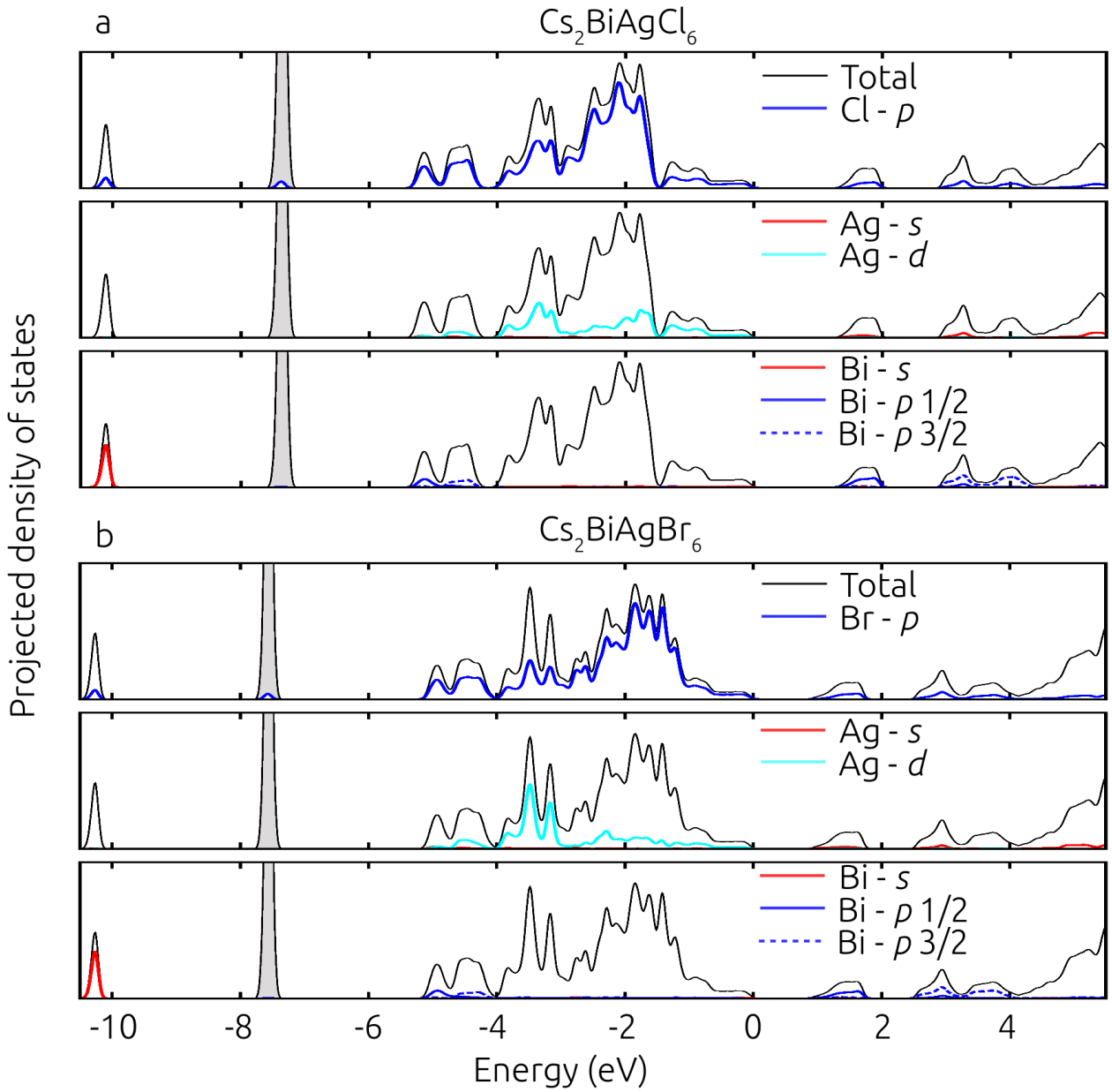

Figure S3: Projected densities of states calculated for $Cs_2BiAgCl_6$ (a) and $Cs_2BiAgBr_6$ (b) within DFT+SOC. The grey shaded peak appearing just above -8 eV in the valence band corresponds to the states localized on the Cs atom. The total density of states is plotted with a black line everywhere. Blue lines correspond to the p states, red lines correspond to the s states and light blue lines correspond to d states. These states are assigned to Bi, Ag, Cl or Br according to the legend. For Bi we distinguish between the spin-orbit split Bi p 1/2 (continuous line) and Bi p 3/2 (dashed line).

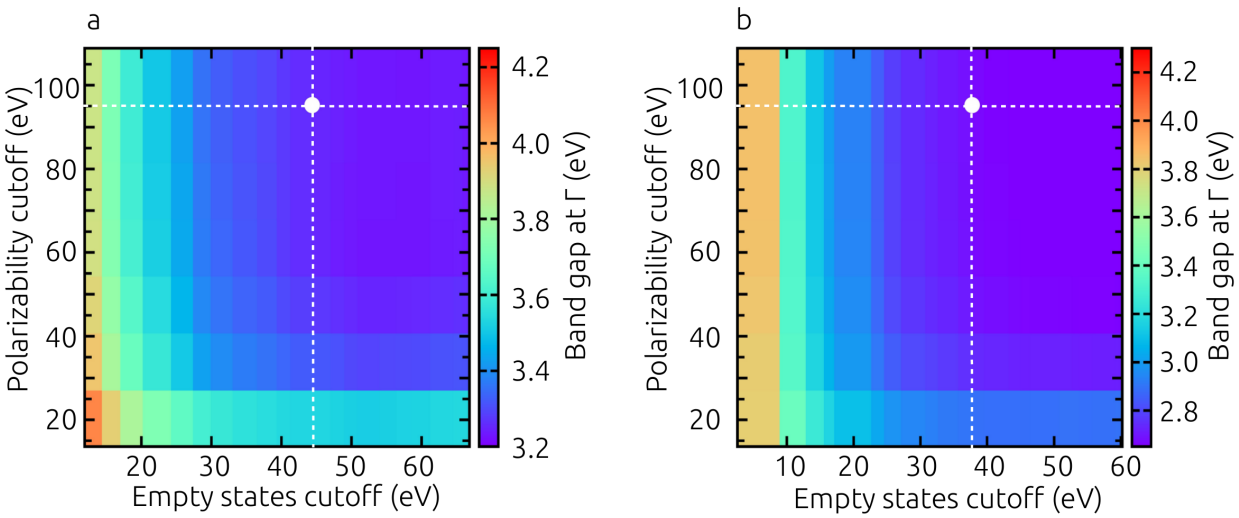

Figure S4: Convergence of the direct band gap at with respect to the empty states cutoff and polarizability cutoff for Cs 2 BiAgCl 6 (a) and Cs 2 BiAgBr 6 (b) . All band gaps are obtained from calculations at Γ-point only. The white dot and dashed white lines highlight the parameters used in our final calculations.

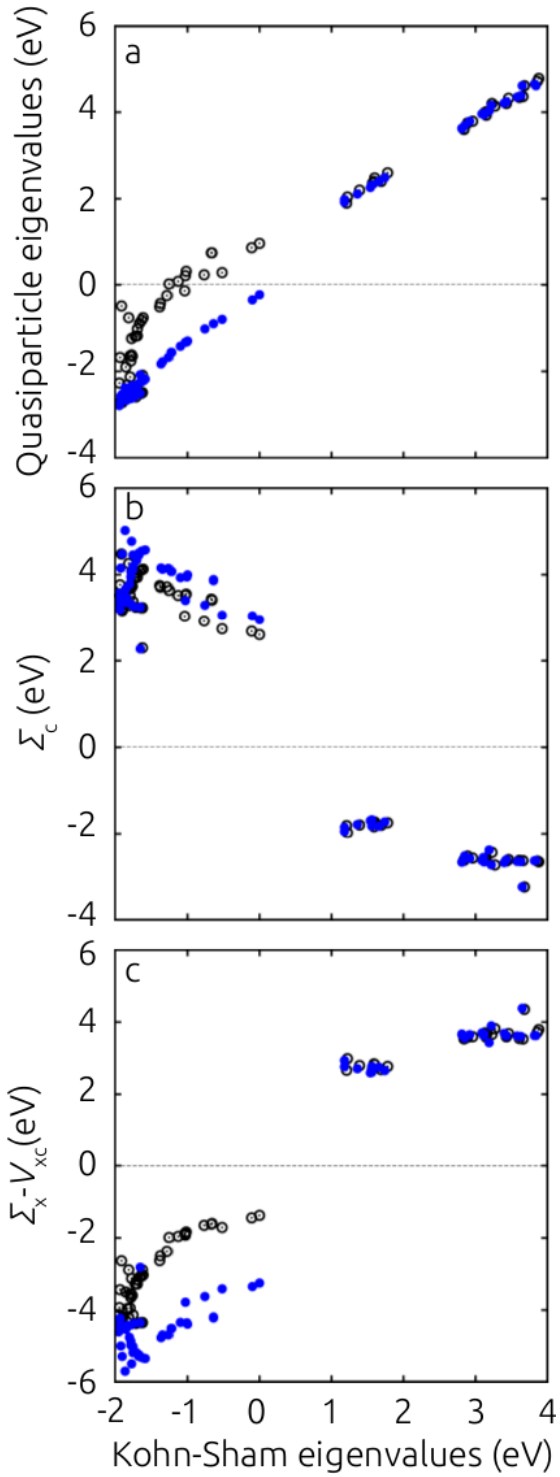

Figure S6: Plot of the quasiparticle energy (a), correlation self energy, Σ_c (b) and the difference between exchange self energy and the exchange-correlation potential, $\Sigma_x - V_{xc}$ (c) with respect to corresponding Kohn-Sham eigenvalues, for calculations without (empty black circles) and with (blue dots) semicore states for Ag. Both calculations are performed for $Cs_2BiAgCl_6$.

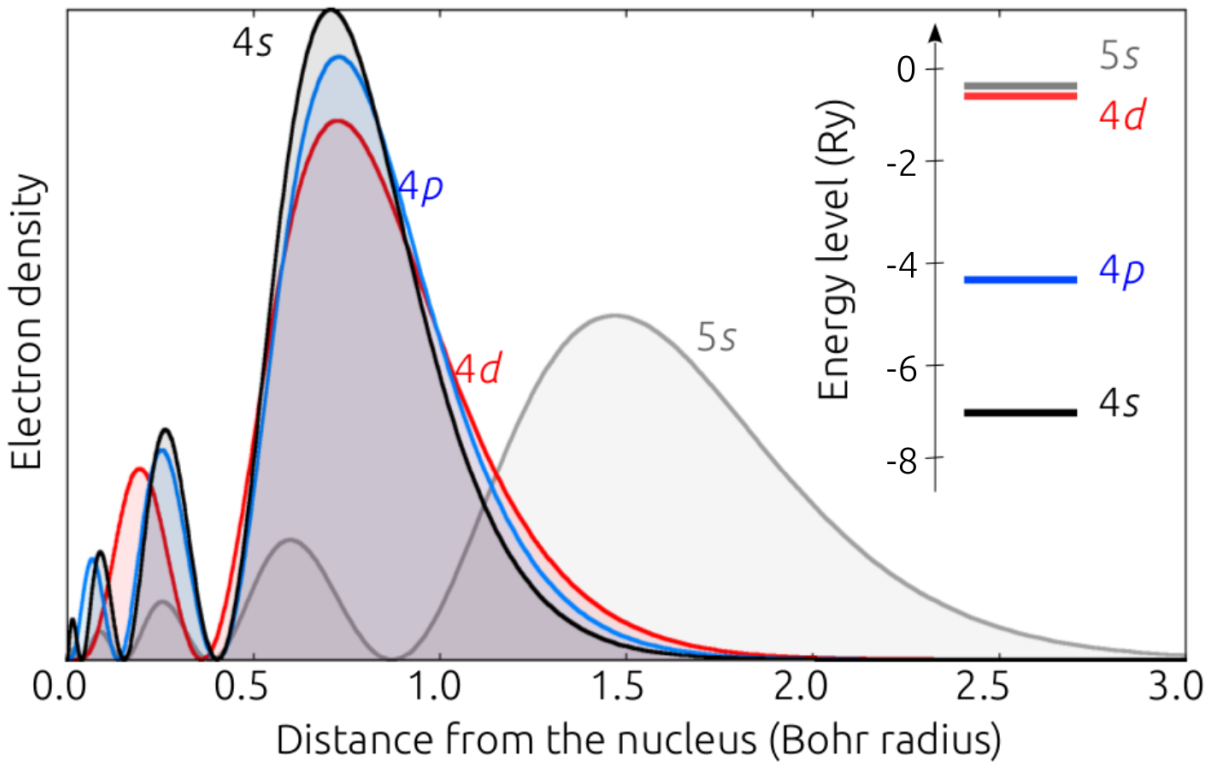

Figure S7: Overlap of the radial part of the $5s$, $4d$, $4p$ and $4s$ pseudo-atomic electron density of Ag as a function of the distance from the nucleus. The inset shows a schematic diagram of the energies of each orbital.

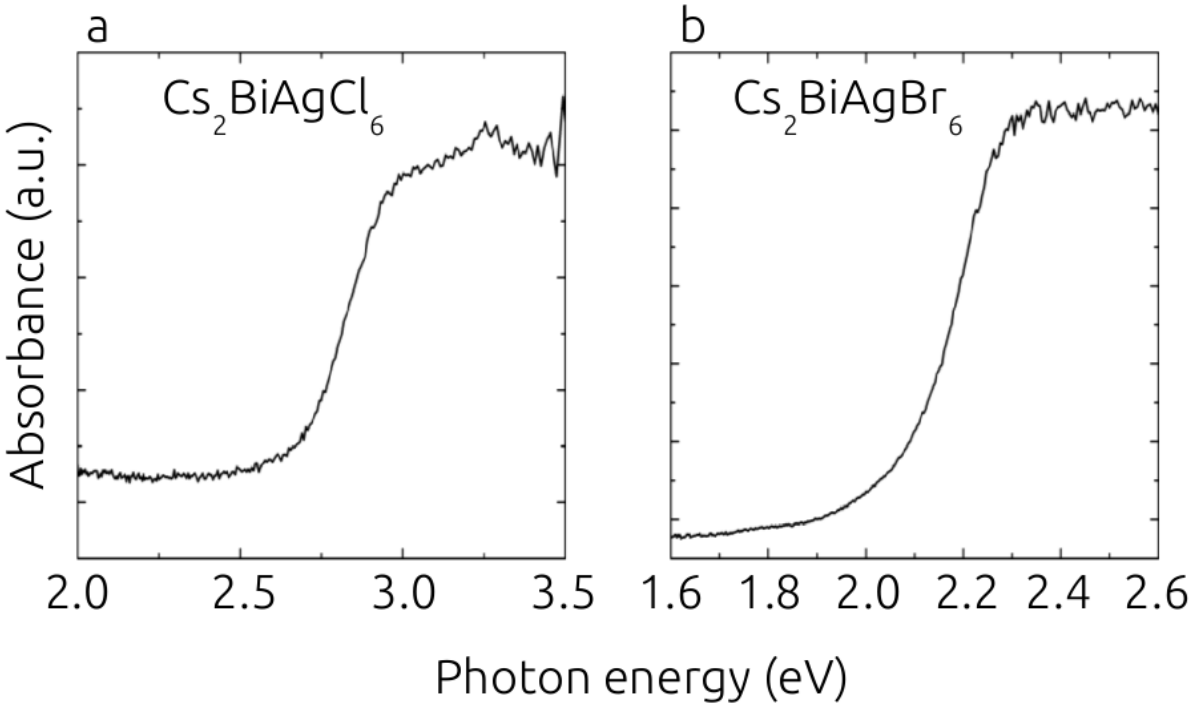

Figure S8: Room temperature optical absorption spectra of $Cs_2BiAgCl_6$ (a) and $Cs_2BiAgBr_6$ (b). The spectrum (a) is the same as the one we reported in Figure 2 of Ref.[16]

References

(1) Perdew, J. P.; Zunger, A. Self-Interaction Correction to Density-Functional Approximations for Many-Electrons Systems. *Phys. Rev. B* **1981**, *23*, 5048.

(2) Gianozzi, P.; Baroni, S.; Bonini, N.; Calandra, M.; Car, R.; Cavazzoni, C.; Ceresoli, D.; Chiarotti, G. L.; Cococcioni, M.; Dabo, I.; Dal Corso, A.; de Gironcoli, S.; Fabris, S.; Fratesi, G.; Gebauer, R. et al. QUANTUM ESPRESSO: A Modular and Open-Source Software Project for Quantum Simulations of Materials. *J. Phys.: Condens. Matter.* **2009**, *21*.

(3) Vanderbilt, D. Soft Self-Consistent Pseudopotentials in a Generalized Eigenvalue Formalism. *Phys. Rev. B* **1990**, *41*, 7892.

(4) Louie, S. G.; Froyen, S.; Cohen, M. L. Nonlinear Ionic Pseudopotentials in Spin-Density-Functional Calculations. *Phys. Rev. B* **1982**, *26*, 1738.

(5) Pseudopotentials. `http://theossrv1.epfl.ch/Main/Pseudopotentials`, accessed: September, 2015.

(6) Troullier, N.; Martins, J. L. Efficient Pseudopotentials for Plane-Wave Calculations. *Phys. Rev. B* **1991**, *43*, 1993.

(7) Hybertsen, M. S.; Louie, S. G. Electron Correlation in Semiconductors and Insulators: Band Gaps and Quasiparticle Energies. *Phys. Rev. B* **1986**, *34*, 5390.

(8) Aryasetiawan, F.; Gunnarsson, O. The *GW* Method. *Rep. Prog. Phys.* **1998**, *61*, 237.

(9) Giustino, F.; Cohen, M. L.; Louie, S. G. *GW* Method with the Self-Consistent Sternheimer Equation. *Phys. Rev. B* **2010**, *81*, 115105.

(10) Onida, G.; Reining, L.; Rubio, A. Electronic Excitations: Density-Functional Versus Many-Body Green's Function Approaches. *Rev. Mod. Phys.* **2002**, *74*, 601–659.

(11) Marini, A.; Hogan, C.; Grüning, M.; Varsano, D. Yambo: An Ab Initio Tool for Excited State Calculations. *Comp. Phys. Commun.* **2009**, *180*, 1392.

(12) Ceperley, D. M.; Alder, B. J. Ground State of the Electron Gas by a Stochastic Method. *Phys. Rev. Lett.* **1980**, *45*, 566.

(13) Adler, S. L. Quantum Theory of the Dielectric Constant in Real Solids. *Phys. Rev.* **1962**, *126*, 413–420.

(14) Godby, R. W.; Needs, R. J. Metal-Insulator Transition in Kohn-Sham Theory and Quasiparticle Theory. *Phys. Rev. Lett.* **1989**, *62*, 1169.

(15) McClure, E. T.; Ball, M. R.; Windl, W.; Woodward, P. M. Cs_2AgBiX_6 (X = Br, Cl): New Visible Light Absorbing, Lead-Free Halide Perovskite Semiconductors. *Chem. Mater.* **2016**, *28*, 1348–1354.

(16) Volonakis, G.; Filip, M. R.; Haghighirad, A. A.; Sakai, N.; Wenger, B.; Snaith, H. J.; Giustino, F. Lead-Free Halide Double Perovskites via Heterovalent Substitution of Noble Metals. *J. Phys. Chem. Lett.* **2016**, *7*, 1254–1259.

(17) Larson, A. C.; Von Drele, R. B. General Structure Analysis System (GSAS). *Los Alamos National Laboratory Report LAUR* **2000**, 86–748.

(18) Sheldrick, G. M. Crystal Structure Refinement with SHELXL. **2015**, *71*, 3.